# Hydrothermal synthesis of Ir and Ir—Pd nanoparticles on carbon nanotubes

*R. V. Borisov,[a,b]★ O. V. Belousov,[a,b] M. N. Likhatski,[a] A. M. Zhizhaev,[a] and S. D. Kirik[a,b]*

[a]*Institute of Chemistry and Chemical Technology, Siberian Branch of the Russian Academy of Sciences, 50/24 Akademgorodok, 660036 Krasnoyarsk, Russian Federation. Fax: +7 (391) 249 4108*
[b]*Siberian Federal University, 79 Svobodnyi prosp., 660041 Krasnoyarsk, Russian Federation. Fax: +7 (391) 244 8625. E-mail: roma_boris@list.ru*

A technique for the formation of Ir and Ir—Pd nanoparticles on carbon nanotubes (CNTs) under hydrothermal conditions was proposed. Reduction of potassium hexachloroiridate(IV) from aqueous solutions with sodium tetrahydroborate in alkaline media at a temperature of 180 °C leads to the formation of iridium nanoparticles on the carbon material. Subsequently, the composite material Ir/CNT was modified by palladium deposition through the decomposition of an alkaline solution of tetraamminepalladium(II) chloride in an autoclave. The composition, dimensions, and structure of the obtained functional materials were characterized by scanning electron microscopy with local energy-dispersive X-ray fluorescence analysis, powder X-ray diffraction, and X-ray photoelectron spectroscopy. The metal particles uniformly coat on the CNTs and have diameters of 5—8 and 15—20 nm in the case of iridium and palladium, respectively.

**Key words:** iridium, palladium, hydrothermal synthesis, carbon nanotubes, surface, catalysts.

In recent years, when studying transition metal compounds, a great deal of attention has been directed towards iridium functional composite nanomaterials, which are actively being used for catalytic applications.[1] Iridium nanoparticles deposited on various materials exhibit high catalytic activity in processes of hydrogenation, dehydrogenation, oxygen evolution and reduction, as well as in aqueous electrolyzers.[1—6] A review[7] of recent advances in the use of iridium-containing catalysts in hydrogenation processes has been published. Iridium nanoparticles are characterized by high activity, selectivity, and the highest resistance to oxidation in air among the platinum group metals. The overall properties and efficiency of iridium catalysts are considerably affected by the size and shape of the particles, the morphology and structure of their surface. A high surface to volume ratio of particles, which can be achieved during synthesis, leads to a decrease in metal consumption and an increase of the number of catalytically active centers.[6—13] An alternate approach toward improving the characteristics of functional materials and increasing the catalytic activity is the addition of other metals.[9,10,14—17] In this case, the key factors include not only the ratio of metals, but also the structure of bi- or polymetallic particles.[10,14,15,17] For example, Pt—Pd and Pt—Ir nanoparticles deposited on carbon exhibit a higher catalytic activity in the oxidation of ammonia compared to the monometallic catalyst Pt/C.[14]

Highly porous carbon materials, such as sibunite, graphene, nanotubes, CMK-3 are widely used as metal carriers.[18—24] These materials have a number of advantages: chemical and thermal stability over a wide temperature range, the possibility of synthesizing high purity samples.[21,22] Among these carriers, carbon nanotubes (CNTs) have low microporosity; therefore, the catalytic process occurs on an external, easily accessible surface, and the substrates should not diffuse into the pores.

There are many methods for the synthesis of iridium metal nanoparticles on supports, including chemical deposition, impregnation with an aqueous solution of complex salts followed by thermal decomposition, electrodeposition, and reduction under radiation.[7,25—30] The synthesis of metal particles in solutions is often accompanied by the introduction of stabilizing reagents that prevent particle aggregation, but, at the same time, can become firmly bound on their surface, reducing the

Published in Russian in *Izvestiya Akademii Nauk. Seriya Khimicheskaya,* No. 6, pp. 1164—1172, June, 2022.
1066-5285/22/7106-1164

catalytic activity of the functional materials.[28] In this regard, the search for simple methods of synthesis of nanoparticles without surface-active additives is of interest to researchers.

Published works[9,31] note that nucleation occurs slowly at low temperatures, which leads to the diffusion of the intermediate products and the formation of large particles. An increase in temperature favors the rapid formation of numerous nuclei of the new phase, thus resulting in smaller nanoparticles.[31] Therefore, it is expedient to obtain platinum group metal nanoparticles on a support under hydrothermal conditions by reduction from complex compounds in aqueous solutions. Carrying out processes in aqueous solutions in closed systems makes it possible to use reagents in stoichiometric amounts, simplifies the standardization of experiments, and eliminates local overheating that can occur during high-temperature decomposition of compounds in a gaseous medium.[32,33] Approaches toward the formation of mono- and bimetallic nanoparticles of non-ferrous and noble metals on oxide and carbon carriers under hydrothermal conditions by the decomposition of various complex compounds and contact reduction reactions were considered in published works.[9,21,32—35] It was found[36] that the kinetic inertness of the reduction of iridium chloride complex compounds, in contrast to platinum and palladium compounds, makes possible the use of a strong reducing agent such as sodium tetrahydroborate without a considerable aggregation of the obtained metal nanoparticles. In this work, this approach is used to develop a one-stage technique of formation of metal nanoparticles on carbon supports without the participation of stabilizers.

The goal of this work is to develop a technique for the formation of nanosized Ir and Ir—Pd metal particles on CNTs under hydrothermal conditions at a temperature of 180 °C.

## Experimental

We used potassium hexachloroiridate(IV) (synthesized according to the procedure described in the work[36]); tetraamminepalladium(II) chloride (synthesized according to the known procedure[32]); hydrochloric acid (high purity grade 20-4); sodium tetrahydroborate (reagent grade); sodium hydroxide (reagent grade), aqueous ammonia (high purity grade 23-5); deionized water prepared using the Direct-Q3 water purification system (Millipore, USA).

Platinum metals were deposited onto Taunit series CNTs,[32,33] which were preliminarily treated for 60 min in an alkaline (0.05 *M* KOH) medium at a temperature of 180 °C in order to clean the surface from residual impurities. Low-temperature nitrogen adsorption isotherms for the materials in question were recorded using an ASAP-2420 analyzer (Micromeritics, USA) at 77 K. Textural characteristics were calculated using the Brunauer—Emmett—Teller (BET) model. According to the results of adsorption measurements, the specific surface area of the material after alkaline treatment and washing with distilled water was 153 $m^2 g^{-1}$, the pore volume was 0.3 $cm^3 g^{-1}$ for an average pore diameter of 7 nm.

The synthesis was carried out in titanium autoclaves with fluoroplastic inserts having a volume of 30 $cm^3$ and quartz autoclaves with a volume of 45 $cm^3$, the design of which was described by us earlier.[32,36]

In order to obtain functional materials Ir/CNT, a carbon support (1 g) weighed with an accuracy of 0.1 mg was placed into an autoclave, potassium hexachloroiridate(IV) solution (10.0 mL), prepared immediately before the experiment by dissolving the required weighed portion of salt in distilled water, and a 0.05 *M* KOH solution (10.0 mL) were added to it. A weighed portion of sodium tetrahydroborate was added to a fluoroplastic cup on the inner surface of the autoclave lid. The autoclave was sealed and heated in an air thermostat in the vertical position for 40 min to 180 °C. After the completion of heating, stirring was turned on, which ensured phase mixing. After 15 min, the autoclave was cooled using running water and unsealed, the solution was filtered to determine the iridium concentration. The precipitate in the form of a black powder was repeatedly washed with hot distilled water. The solid phase was precipitated in a CR4000 centrifuge (Centurion Scientific, Great Britain) for 15 min at 4000 rpm. The precipitates were vacuum dried to constant weight at a temperature of 80 °C.

For the deposition of palladium on the obtained Ir/CNT material, a weighed portion of the Ir/CNT material was placed in a fluoroplastic reactor, a specific amount of tetraamminepalladium(II) chloride was added, a 0.05 *M* KOH solution (20 $cm^3$) was poured inside, and the system was sealed. The reaction mass was stirred for 15 min at 25 °C, after which the autoclave was placed in a thermostat heated to 180 °C for 120 min with constant rotation in the vertical plane. After the completion of the experiment, the autoclave was unsealed, the solution was removed for analysis, and the solid phase was repeatedly washed with hot distilled water and vacuum dried at 80 °C.

X-ray diffraction patterns were recorded in the range of angles $2\theta = 5—90°$ with a step of 0.02° on an X′Pert Pro diffractometer (Panalytical, Netherlands) using Cu-$K\alpha_1$-radiation ($\lambda = 0.15418$ nm). The morphological features of the precipitated particles were studied by scanning electron microscopy (SEM) on scanning electron microscopes S5500 (Hitachi, Japan) and TM4000Plus (Hitachi, Japan) with a Quantax 150 microanalysis system (Bruker, Germany). X-ray photoelectron spectra were recorded on a SPECS spectrometer (Germany) equipped with a PHOIBOS 150 MCD-9 hemispherical energy analyzer; monochromatic Al-Kα radiation from an X-ray tube anode (1486.6 eV) with an energy analyzer transmission energy of 20 eV for survey spectra and 10 eV for high-resolution spectra was used for excitation. The spectra were processed using the CasaXPS

software. The surface of the samples was etched with $Ar^+$ ions for 5 min at an accelerating voltage of 5 kV and an ion emission current of 30 μA. After subtracting the nonlinear Shirley background, the spectra of Pd $3d_{5/2,3/2}$ and Ir $4f_{7/2,5/2}$ were approximated by doublets with Gauss—Lorentz form components with a spin-orbit splitting of 5.3 and 3.0 eV and an intensity ratio of 0.67 and 0.75, respectively.

The chemical element content in solutions was determined by inductively coupled plasma mass spectrometry on an Agilent 7900 instrument (Agilent, USA).

Electrochemical studies with a linear potential sweep were carried out using an EC301 potentiostat (Stanford Research System, USA) using three-electrode configuration. A platinum wire was used as the counter electrode, a saturated silver chloride electrode served as the reference electrode, relative to which, after taking into account the ohmic voltage drop, all potentials were measured. A 0.5 *M* $H_2SO_4$ solution was used as the supporting electrolyte, the potential sweep rate was 20 mV $s^{-1}$, the sweep direction was from the cathode region to the anode one. The working electrode was prepared by placing a weighted portion of the material (10.0 mg) with or without deposited metal nanoparticles into a platinum cup. All the measurements were carried out in air at a temperature of 25 °C and atmospheric pressure.

## Results and Discussion

In a previous work[36] we determined the characteristics of iridium nanoparticles formed in the reduction of aqueous solutions of potassium hexachloroiridate(IV) with sodium tetrahydroborate under hydrothermal conditions. In this work, the obtained[36] dependencies were used to develop a one-stage hydrothermal method for the preparation of iridium nanoparticles on the surface of a carbon material.

In an alkaline medium, the reduction process can be schematically represented as follows:

$$2\,K_2IrCl_6 + NaBH_4 + 3\,KOH = \\ = 2\,Ir + H_3BO_3 + 7\,KCl + NaCl + 4\,HCl. \qquad (1)$$

Synthesis temperature was 180 °C. In this case, in contrast to synthesis at lower temperatures, we expect the formation of numerous nuclei of the new phase, therefore, it is possible to obtain smaller particles.[31] Taking into account the quantitative reduction of potassium hexachloroiridate(IV) with sodium tetrahydroborate under these conditions, materials with a specified metal content can be synthesized within 5—15 min (Table 1). After the completion of the experiments, the concentration of iridium ions in the solution did not exceed 0.01 mg $L^{-1}$, which corresponds to a degree of metal reduction of more than 99%.

The deposition of the required amount of palladium on the formed Ir/CNT materials can be carried out using autoclave thermolysis.[32] At a temperature of 180 °C in an aqueous solution of potassium hydroxide, tetraamminepalladium(II) chloride is quantitatively reduced with the formation of metal nanoparticles (Eq. (2)), which are evenly distributed over the carbon support surface.[32] In this case, Ir—Pd/CNT samples with various metal contents were obtained (see Table 1).

$$3\,[Pd(NH_3)_4]Cl_2 + 6\,KOH \longrightarrow \\ \longrightarrow 3\,Pd + N_2 + 10\,NH_3 + 6\,H_2O + 6\,KCl \qquad (2)$$

The study of the synthesized materials by SEM showed (Fig. 1, *a*—*c*) that iridium particles with an almost spherical shape form on the CNTs. Depending on the iridium content on the surface, the average particle diameter ranged from 5 to 8 nm. An increase in the proportion of iridium from 1.0 to 6.4 wt.% leads to the formation of aggregated particles with sizes of 10—15 nm, which consist of smaller globules.

According to SEM, in the presence of tetraamminepalladium(II) chloride, following decomposition (Fig. 1, *d*), the CNTs in the autoclave contain, in addition to the previously deposited iridium particles, spherical particles with sizes greater than 15 nm. The particle size distribution (see Fig. 1) is broader compared to that of monometallic samples. Despite the fact that palladium tends to form large particles, it can also be present in the form of finer particles. Local X-ray microfluorescence analysis (Fig. 2, Table 2) showed

**Table 1.** Formation conditions and composition of composite materials, $T = 180$ °C

| Synthesis conditions | Composite material | Contents of metals (wt.%) | |
|---|---|---|---|
| | | Ir | Pd |
| Reduction of $K_2IrCl_6$ with sodium tetrahydroborate in solution (0.05 *M* KOH + 0.01 *M* $NH_4OH$), τ = 15 min | Ir/CNT-1 | 1.0 | – |
| | Ir/CNT-2 | 2.0 | – |
| | Ir/CNT-3 | 5.0 | – |
| | Ir/CNT-4 | 6.4 | – |
| Decomposition of $[Pd(NH_3)_4]Cl_2$ in solution 0.05 *M* KOH, τ = 120 min | Ir-Pd/CNT-5 | 4.8 | 4.8 |
| | Ir-Pd/CNT-6 | 1.0 | 1.0 |

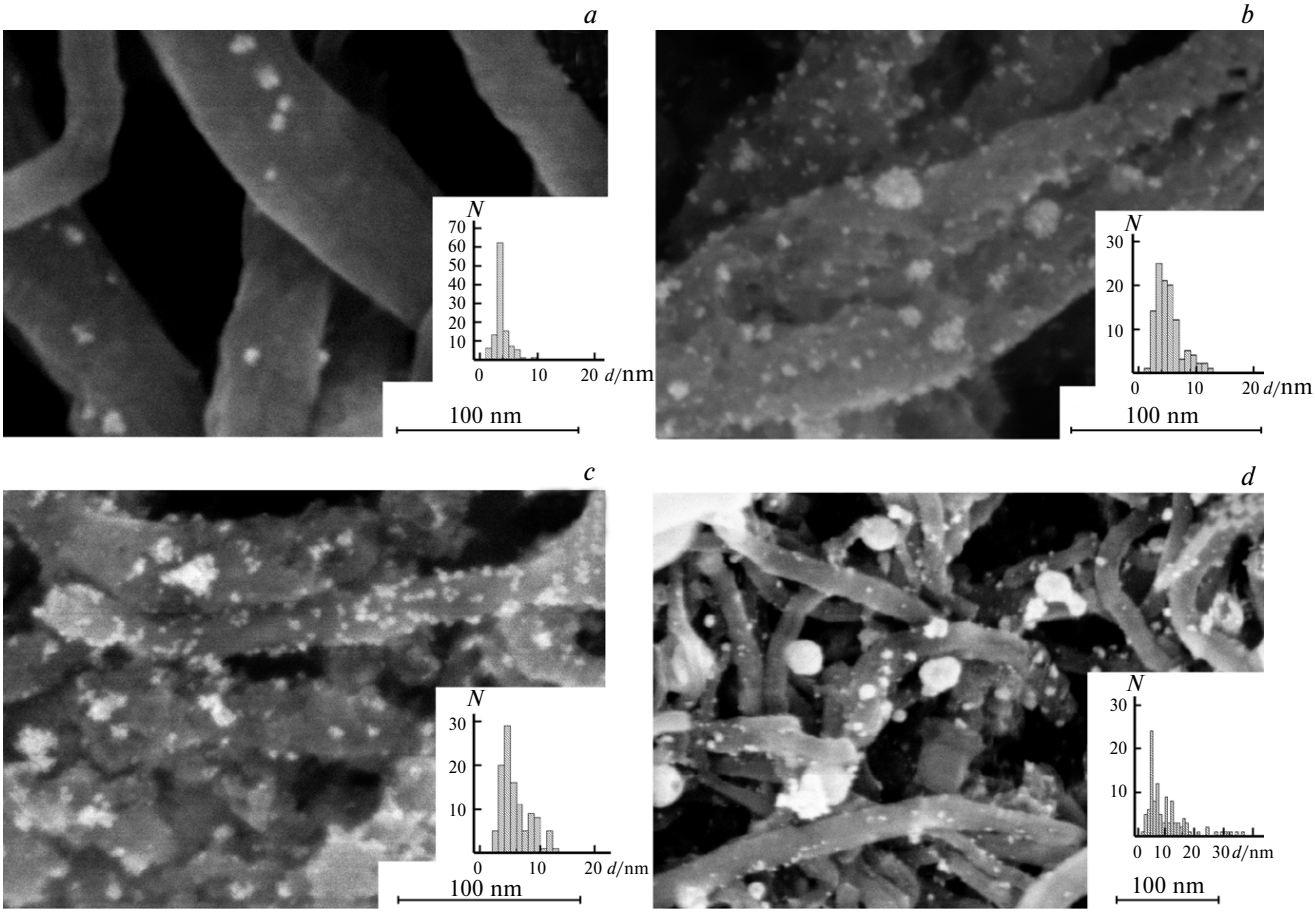


**Fig. 1.** SEM images of particles deposited on CNTs: *a*, Ir/CNT, 1.0 wt.%; *b*, Ir/CNT, 5.0 wt.%; *c*, Ir/CNT, 6.4 wt.%; *d*, Ir—Pd/CNT, Ir, 4.8 wt.%; Pd, 4.8 wt.%; insets show the particle size distribution.

that the Ir—Pd/CNT-5 material contains C, Pd, and Ir atoms (the Al signal corresponds to the sample holder). Platinum metals are evenly distributed over the support with a mass ratio close to 1 : 1, which corresponds to the sample composition according to the synthesis conditions. Similar dependencies are observed for a material with a lower metal content (Ir—Pd/CNT-6), with the sizes of palladium particles shifting slightly toward smaller diameters.

The crystal structure of Ir/CNT was determined by powder X-ray diffraction (Fig. 3). The X-ray diffraction pattern shows a peak of the carbon support phase at $2\theta = 26°$, corresponding to a graphite-like structure, and a weak peak at $2\theta = 43°$, overlapping with the iridium peaks. In the case of materials with an iridium content of 2.0 wt.% or more, we observed weak reflections ($2\theta = 40.8°$) in the direction of the plane (111), which are characteristic of metallic iridium. The remaining reflections ($2\theta = 47.5°$ and 69.4°) are practically unnoticeable due to low metal content and small particle size. Peak broadening can be used to estimate the size of the coherent scattering region (CSR) $d$ by the Scherrer formula (I):

$$d = K\lambda/(\beta\cos\theta), \quad \text{(I)}$$

where $K$ is the particle shape factor, which is equal to 0.89;[34] $\lambda$ is the radiation wavelength (0.15418 nm); $\beta$ is the peak width at half maximum; $\theta$ is the position of the peak (deg). For the Ir/CNT-3 sample (see Table 1), the CSR size was 4.5 nm, which is in good agreement with the diameters of particles determined using electron microscopy results.

The diffraction pattern of the Ir—Pd/CNT-5 sample (see Fig. 3) shows reflections characteristic of metallic palladium corresponding to the planes (111) and (200) at $2\theta = 40.1°$ and 46.7°, respectively. The formation of solid solutions Ir—Pd was not observed. The crystallite sizes were estimated using the splitting of the peak (111) into two components (corresponding to palladium and iridium). The CSR size for iridium and palladium was 4.5 and 5.4 nm, respectively. This fact indirectly confirms the formation of fine palladium parti-

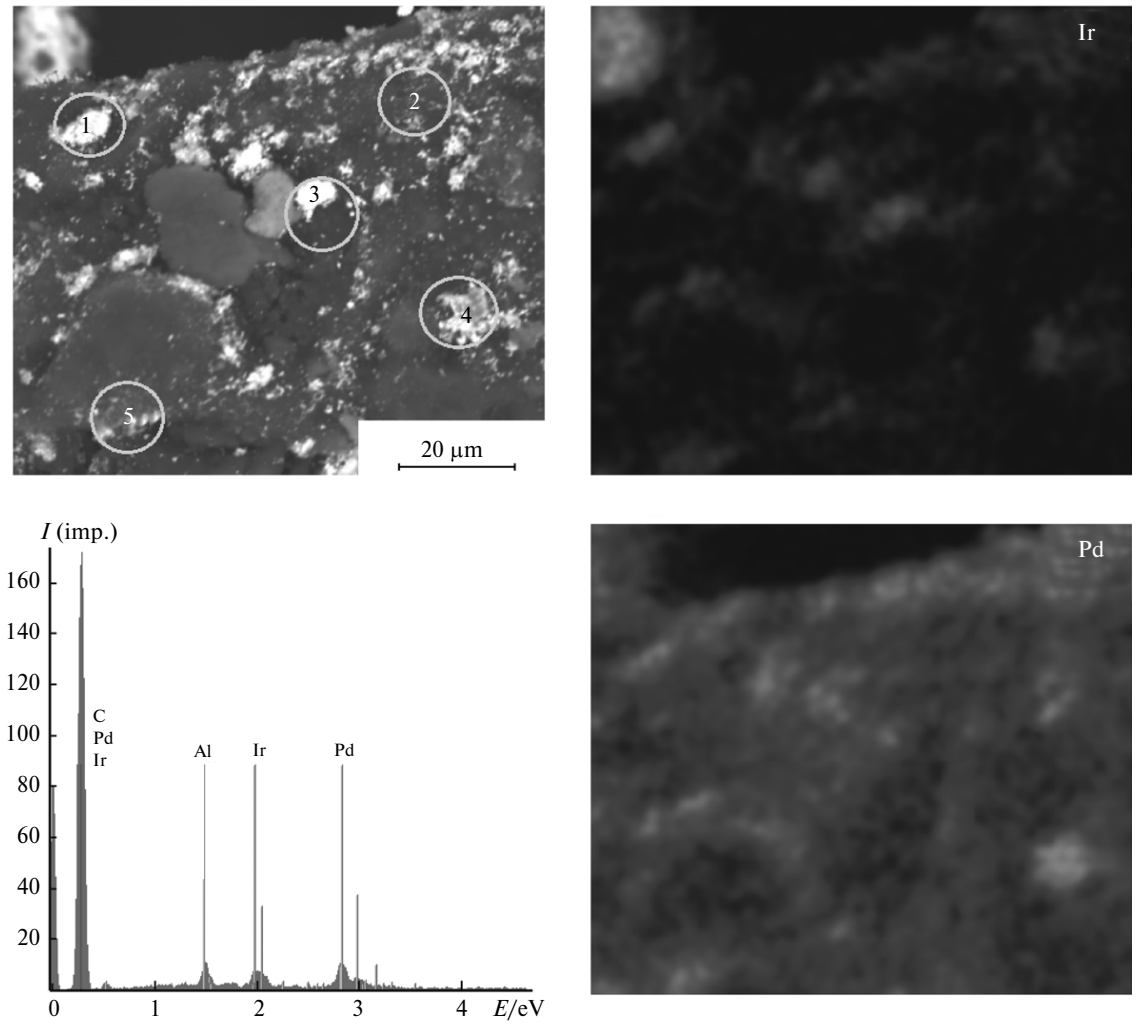


**Fig. 2.** Results of local X-ray microfluorescence analysis of sample Ir—Pd/CNT (Ir, 4.8 wt.%; Pd, 4.8 wt.%).

cles. At the same time, the sizes of palladium crystallites are smaller than the diameters of particles estimated using microscopy results, therefore, it can be assumed that palladium in this case has a multiblock structure, in which a single particle consists of several crystallites.

**Table 2.** Metal content at various points (see Fig. 2, *a*) according to X-ray microanalysis of sample Ir—Pd/CNT (Ir, 4.8 wt.%; Pd, 4.8 wt.%)

| Region | *C* (wt.%) | |
|---|---|---|
| | Ir | Pd |
| 1 | 46.3 | 53.7 |
| 2 | 57.0 | 43.0 |
| 3 | 64.5 | 35.5 |
| 4 | 52.3 | 47.7 |
| 5 | 51.3 | 48.7 |

Figure 4 shows the X-ray photoemission spectra of the synthesized materials Ir/CNT (5.0 wt.%) and Ir—

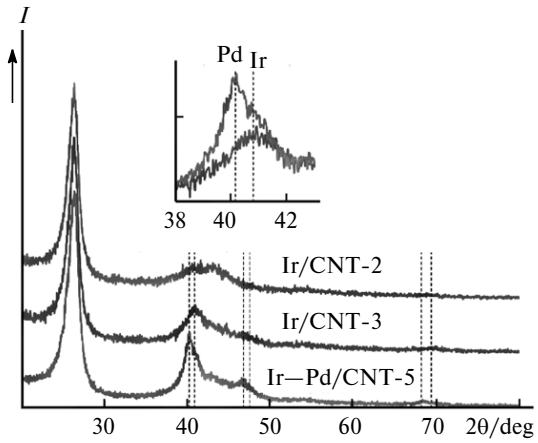


**Fig. 3.** Fragments of sample diffraction patterns (see Table 1); the inset compares the shapes of peaks (111) for samples Ir/CNT (5.0 wt.% Ir) and Ir—Pd/CNT (Ir, 4.8 wt.%; Pd, 4.8 wt.%).

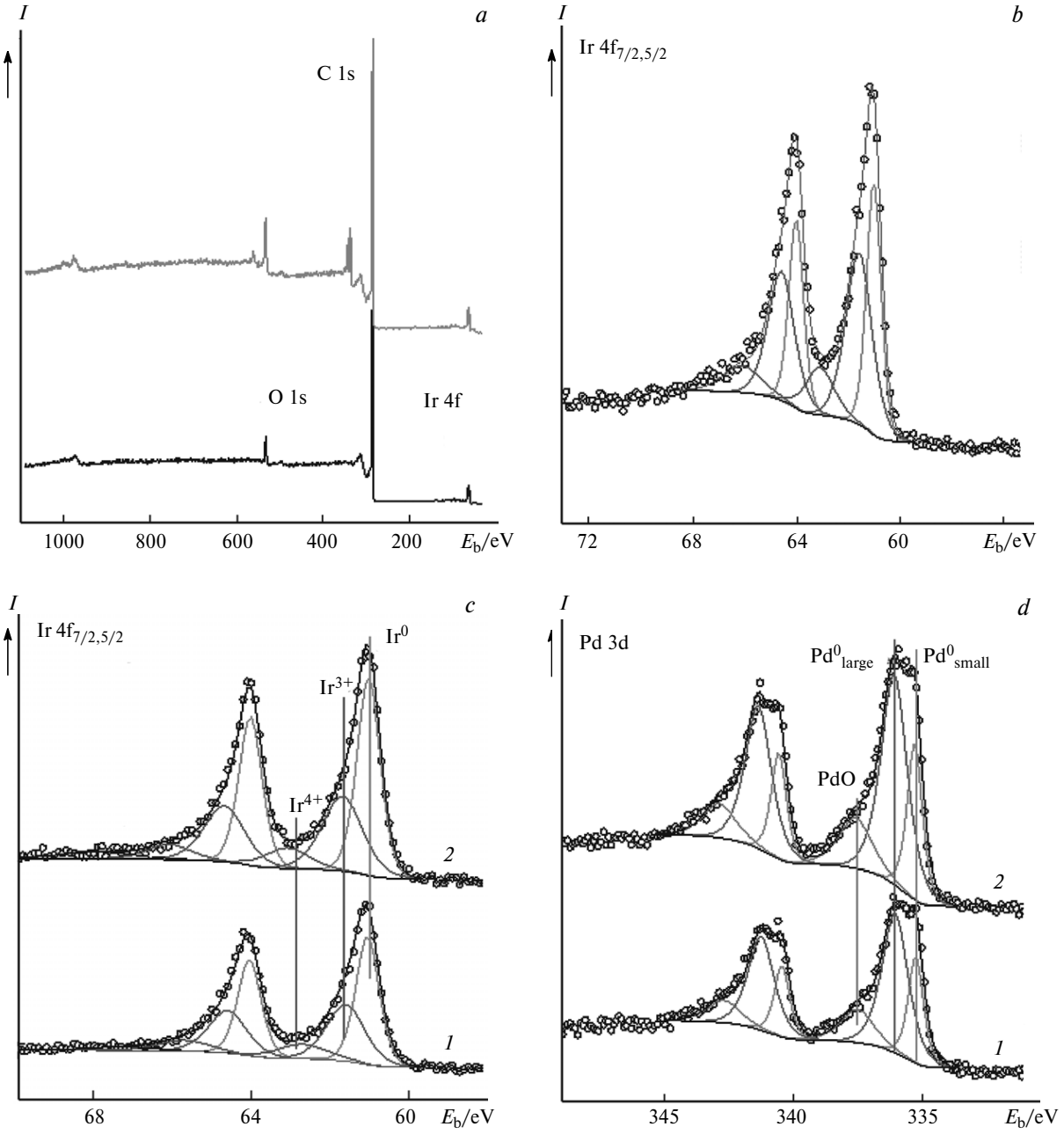


**Fig. 4.** X-ray photoelectron spectra for a wide range of binding energies (*a*), as well as high resolution spectra of Ir/CNT-3 (*b*) and Ir—Pd/CNT-5 (*c*, *d*) before (*1*) and after ion treatment (*2*); $E_b$ is the binding energy. Lines $Pd^0_{large}$ and $Pd^0_{small}$ correspond to large and small $Pd^0$ particles, respectively.

Pd/CNT (Ir, 4.8 wt.%; Pd, 4.8 wt.%). The survey spectrum (see Fig. 4, *a*) of the carbon material after the reduction of potassium hexachloroiridate(IV) in an autoclave contains Ir $4f_{7/2,5/2}$, C 1s, and O 1s lines. The absence of the Cl 1s line at a binding energy of ~200 eV implies a high degree of purification of the resulting composite from unreduced iridium(IV) chlorocomplexes.

After the deposition of palladium on this material, the contribution of the oxygen line increases somewhat, while that of the C 1s line decreases, which can be related to both the partial oxidation of the carbon support and the coating of the surface with $Pd^0$ particles. The change in the relative atomic concentration of iridium is negligible. This allows us to exclude the possibility of the iridium particles becoming coated with a layer of palladium, *i.e.*, the formation of core—shell structures.

Analysis of high-resolution spectra showed that the Ir 4f line can be deconvoluted into three components

(see Fig. 4, *b*), which, in order of increasing binding energy, belong to metallic iridium $Ir^0$ particles, as well as to oxidized forms $Ir^{III}$ and $Ir^{IV}$.[36–38] Due to the absence of chlorine lines in the spectrum, the oxidized forms of iridium can be attributed to the corresponding oxide compounds. The fraction of metallic iridium on the surface of the Ir/CNT-3 sample was 50%, and, after the addition of palladium (Ir—Pd/CNT-5 sample), it increased to 60%, which is related to the probable post-reduction of oxide forms. Apparently, the high quantity of oxidized species of iridium on the surface of the composite material compared to that of pure iridium nanopowders[36] is due to small particle sizes and, as a result, high specific surface areas.

The Pd 3d line in the spectrum of the Ir—Pd/CNT-5 sample can be represented by three components (see Fig. 4, *d*), two of which are assigned to metal particles with different degrees of dispersity,[39] while the line with the binding energy Pd $3d_{5/2}$ (337.5 eV) corresponds to the oxidized species of palladium(II).[40] It can be inferred from the ratio of the components of the Pd 3d line that the deposition of palladium occurs predominantly (>90%) in the form of metal nanoparticles. The presence of two components in the spectra of the Pd $3d_{5/2,3/2}$ line corresponding to metallic palladium may be related to the bimodal particle size distribution, with one of the fractions exhibiting a considerable chemical shift.[39] This supposition is consistent with the particle size distribution obtained using SEM results (see Fig. 1, *d*). According to XPS results, the contribution of small particles is about 25%, while that of large particles is more than 65%.

Etching of the Ir—Pd/CNT-5 sample with $Ar^+$ ions for 5 min (see Fig. 4, *c*, *d*) is accompanied by a slight increase in the intensity of the Pd 3d and Ir 4f lines, which may be related to the predominant removal of lighter carbon atoms. At the same time, the ratio of oxidized and metallic species of both iridium and palladium remains practically unchanged.

Platinum group metals exhibit catalytic properties during the anodic oxidation of water.[41,42] Figure 5 shows the polarization curves of the starting carbon nanomaterial and that of the material following the deposition of metal nanoparticles. Electrodes with metal nanoparticles deposited on CNTs demonstrate an increase in the current of anodic oxidation of water. In addition, in all the cases involving functional materials, a decrease of overvoltage of electrolytic oxygen evolution is observed. A comparison of polarization curves *2* and *3* (see Fig. 5) allows us to infer that a decrease in the amount of iridium in the material leads to an increase of the current, *i.e.*, to improved catalytic properties.

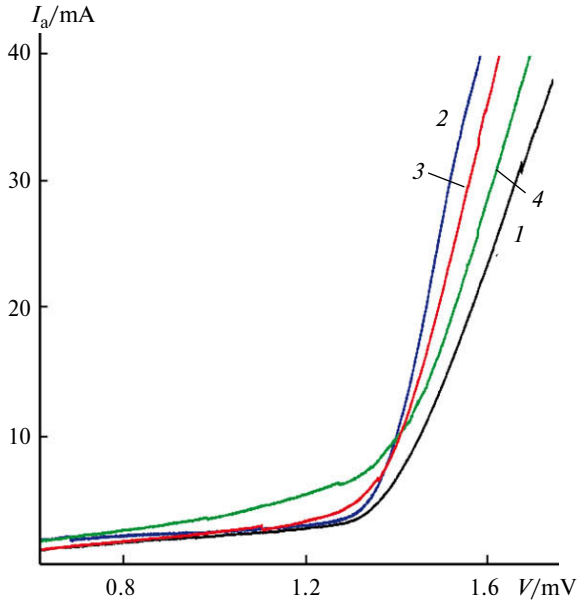


**Fig. 5.** Polarization curves with the linear potential sweep direction toward the anode: *1* — starting carbon nanomaterial; *2* — Ir/CNT (1.0 wt.% Ir); *3* — Ir/CNT (5.0 wt.% Ir); *4* — Ir—Pd/CNT (Ir, 4.8 wt.%; Pd, 4.8 wt.%); *V* is the potential, $I_a$ is the anodic oxidation current.

This effect may be due to the presence of smaller particles and their morphology, in which the active centers are evenly distributed over the carrier and do not aggregate. When a second metal, namely palladium, is added to the functional material, a decrease in catalytic activity is observed, which is probably due to the presence of large palladium particles (15—20 nm), which can block the catalytically active iridium centers.

In conclusion, a hydrothermal autoclave method for the preparation of Ir and Ir—Pd nanoparticles on a carbon material with a specified quantitative ratio has been proposed. The formation of iridium particles with sizes of 5—8 nm occurs during the reduction of aqueous solutions of potassium hexachloroiridate(IV) with sodium tetrahydroborate in an alkaline medium at a temperature of 180 °C for 15 min. Autoclave decomposition of an alkaline solution of tetraamminepalladium(II) chloride can be used to add palladium nanoparticles to the composite material Ir/CNT. X-ray microfluorescence analysis showed that metal particles are evenly distributed over the carrier surface. X-ray photoelectron spectroscopy was used to demonstrate that iridium on the surface of CNTs is represented by species with the oxidation states 0, 3+, and 4+, while palladium is predominantly in the form of a metal. The obtained functional materials were found to have positive catalytic effects in processes of anodic oxidation of water compared to that of the starting CNTs.

This research was carried out in accordance with the state assignment of the Institute of Chemistry and Chemical Technology of the Siberian Branch of the Russian Academy of Sciences (Project No. 0287-2021-0014) using the equipment of the Krasnoyarsk regional center for collective use FRC KSC SB RAS.

No human or animal subjects were used in this research.

The authors declare no competing interests.

## References

1. B. Huang, Y. Zhao, *EcoMat*, 2022, **e12176**; DOI: 10.1002/eom2.12176.
2. P. Jovanovič, N. Hodnik, F. Ruiz-Zepeda, I. Arčon, B. Jozinović, M. Zorko, M. Bele, M. Šala, V. S. Šelih, S. Hočevar, M. Gaberšček, *J Am. Chem. Soc.*, 2017, **139**, 12837; DOI: 10.1021/jacs.7b08071.
3. F. Lv, J. Feng, K. Wang, Z. Dou, W. Zhang, J. Zhou, C. Yang, M. Luo, Y. Yang, Y. Li, P. Gao, S. Guo, *ACS Cent. Sci.*, 2018, **4**, 1244; DOI: 10.1021/acscentsci.8b00426.
4. H. Over, *ACS Catal.*, 2021, **11**, 8848; DOI: 10.1021/acscatal.1c01973.
5. F Wang, K. Kusada, D. Wu, T. Yamamoto, T. Toriyama, S. Matsumura, Y. Nanba, M. Koyama, H. Kitagawa, *Ang. Chemie*, *Int. Ed.*, 2018, **57**, 4505—4509; DOI: 10.1002/anie.201800650.
6. D. Liu, X. Chen, G. Xu, J. Guan, Q. Cao, B. Dong, Y. Qi, C. Li, X. Mu, *Sci. Rep.*, 2016, **6**, 21365; DOI: 10.1038/srep21365.
7. L. M. Martínez-Prieto, I. Cano, P. W. van Leeuwen, *Top. Organomet. Chem.*, 2021, **69**, 397; DOI: 10.1007/3418_2020_60.
8. X. Kang, Y. Li, M. Zhu, R. Jin, *Chem. Soc. Rev.*, 2020, **49**, 6443; DOI: 10.1039/C9CS00633H.
9. M. Rueping, R. M. Koenigs, R. Borrmann, J. Zoller, T. E. Weirich, J. Mayer, *Chem. Mater.*, 2011, **23**, 2008; DOI: 10.1021/cm1032578.
10. X. Xia, L. Figueroa-Cosme, J. Tao, H. C. Peng, G. Niu, Y. Zhu, Y. Xia, *J Am. Chem. Soc.*, 2014, **136**, 10878; DOI: 10.1021/ja505716v.
11. T. S. Rodrigues, A. G. da Silva, P. H. Camargo, *J. Mater. Chem. A*, 2019, **7**, 5857; DOI: 10.1039/C9TA00074G.
12. J. Feng, F. Lv, W. Zhang, P. Li, K. Wang, C. Yang, B. Wang, Y. Yang, J. Zhou, F. Lin, G.-C. Wang, S Guo., *Adv. Mater.*, 2017, **29**, 1703798; DOI:10.1002/adma.201703798.
13. K. D. Gilroy, X. Yang, S. Xie, M. Zhao, D. Qin, Y. Xia, *Adv. Mater.*, 2018, **30**, 1706312; DOI: 10.1002/adma.201706312.
14. T. L. Lomocso, E. A. Baranova, *Electrochimica Acta*, 2011, **56**, 8551; DOI: 10.1016/j.electacta.2011.07.041.
15. N. A. Bumagin, *Russ. Chem. Bull.*, 2021, **70**, 1483; DOI: 10.1007/s11172-021-3243-y.
16. F. Sanchez, L. Bocelli, D. Motta, A. Villa, S. Albonetti, N. Dimitratos, *Appl. Sci.*, 2020, **10**, 1752; DOI: 10.3390/app10051752.
17. N. A. Bumagin, *Russ. Chem. Bull.*, 2021, **70**, 2034; DOI: 10.1007/s11172-021-3314-0.
18. M. Hara, R. Badam, G. J. Wang, H. H. Huang, M. Yoshimura, *ECS Transactions*, 2018, **85**, 27; DOI: 10.1149/08511.0027ecst.
19. H. Bernas, I. Simakova, I. P. Prosvirin, P. Mäki-Arvela, R. Leino, D. Y. Murzin, *Catal. Lett.*, 2012, **142**, 690; DOI: 10.1007/s10562-012-0809-1.
20. Y. V. Ioni, S. E. Lyubimov, A. A. Korlyukov, M. Y. Antipin, V. A. Davankov, S. P. Gubin, *Russ. Chem. Bull.*, 2012, **61**, 1825; DOI: 10.1007/s11172-012-0252-x.
21. O. V. Belousov, V. E. Tarabanko, R. V. Borisov, I. L. Simakova, A. M. Zhyzhaev, N. Tarabanko, V. G. Isakova, V. Parfenov, I. V. Ponomarenko, *React. Kinet. Mech. Catal.*, 2019, **127**, 25; DOI: 10.1007/s11144-018-1430-0.
22. J. V. Rojas, C. H. Castano, *J. Nanoparticle Res.*, 2014, **16**, 2567; DOI: 10.1007/s11051-014-2567-z.
23. E. S. Kobeleva, D. A. Nevostruev, M. N. Uvarov, D. E. Utkin, V. A. Zinoviev, O. A. Gurova, M. S. Kazantzev, K. M. Degtyarenko, A. V. Kulikova, L. V. Kulik, *Russ. Chem. Bull.*, 2021, **70**, 2427; DOI: 10.1007/s11172-021-3363-4.
24. A. V. Okhokhonin, K. O. Tokmakova, T. S. Svalova, A. I. Matern, A. N. Kozitsina, *Russ. Chem. Bull.*, 2021, **70**, 1191; DOI: 10.1007/s11172-021-3204-5.
25. S. Kundu, H. Liang, *J. Coll. Int. Sci.*, 2011, **354**, 597; DOI: 10.1016/j.jcis.2010.11.032.
26. A. Goel, N. Rani, *Open J. Inorg. Chem.*, 2012, **2**, 67; DOI: 10.4236/ojic.2012.23010.
27. R. Zhang, X. Liu, L. Shi, X. Jin, Y. Dong, K. Li, X. Zhao, Q. Li, Y. Deng, *Nanomaterials*, 2019, **9**, 76; DOI: 10.3390/nano9010076.
28. H. Pu, H. Dai, T. Zhang, K. Dong, Y. Wang, Y Deng, *Current Opinion in Electrochemistry*, 2022, **22**, 100927; DOI: 10.1016/j.coelec.2021.100927.
29. S. V. Saikova, T. V. Trofimova, A. Yu. Pavlikov, D. V. Karpov, D. I. Chistyakov, Yu. L. Mikhlin, *Russ. Chem. Bull.*, 2020, **69**, 1284; DOI:10.1007/s11172-020-2899-z.
30. K. V. Mkrtchyan, A. A. Zezin, E. A. Zezina, S. S. Abramchuk, I. A. Baranova, *Russ. Chem. Bull.*, 2020, **69**, 1731; DOI: 10.1007/s11172-020-2956-7.
31. X. Xia, S. Xie, M. Liu, H. C. Peng, N. Lu, J. Wang, M. J. Kim, Y. Xia, *PNAS*, 2013, **110**, 6669; DOI: 10.1073/pnas.1222109110.
32. R. V. Borisov, O. V. Belousov, A. M. Zhizhaev, *Russ. J. Inorg. Chem.*, 2020, **65**, 1623; DOI: 10.1134/S0036023620100034.
33. R. V. Borisov, O. V. Belousov, A. M. Zhizhaev, M. N. Likhatski, N. V. Belousova, *Russ. Chem. Bull.*, 2021, **70**, 1474; DOI: 10.1007/s11172-021-3242-z.
34. E. N. Tupikova, I. A. Platonov, D. S. Khabarova, *Kinet. Catal.*, 2019, **60**, 366; DOI: 10.1134/S0023158419030145.

35. E. V. Fesik, T. M. Buslaeva, T. I. Melnikova, L. S. Tarasova, A. V. Laptenkova, *Russ. J. Phys. Chem. A.*, 2019, **93**, 1011; DOI: 10.1134/S0036024419060098.
36. R. V. Borisov, O. V. Belousov, A. M. Zhizhaev, S. D. Kirik, Y. L. Mikhlin, *Inorg. Materials*, 2022, **58**, 215; DOI: 10.1134/S0020168522020030.
37. H. E. Rizk, N. E. El-Hefny, *J. Alloys Compd.*, 2020, **812**, 152041; DOI: 10.1016/j.jallcom.2019.152041.
38. F. Claudel, L. Dubau, G. Berthomé, L. Solà-Hernández, C. Beauger, L. Piccolo, F. Maillard, *ACS Catalysis*, 2019, **9**, 4688; DOI: 10.1021/acscatal.9b00280.
39. W. P. Zhou, A. Lewera, R. Larsen, R. I. Masel, P. S. Bagus, A. Wieckowski, *J. Phys. Chem. B*, 2006, **110**, 13393; DOI: 10.1021/jp061690h.
40. A. Felten, J. Ghijsen, J.-J. Pireaux, W. Drube, R. L. Johnson, D. Liang, M. Hecq, G. van Tendeloo, C. Bittencourt, *Micron*, 2009, **40**, 74; DOI: 10.1016/j.micron.2008.01.013.
41. J. Islam, S. K. Kim, H. S. Cho, M. J. Kim, W. C. Cho, C. H. Kim, *Electrochem. Commun.*, 2020, **121**, 106877; DOI: 10.1016/j.elecom.2020.106877.
42. Y. Wen, P. Chen, L. Wang, S. Li, Z. Wang, J. Abed, X. Mao, Y. Min, C. Thang Dinh, P. de Luna, R. Huang, L. Zhang, L. Wang, L. Wang, R. J. Nielsen, H. Li, T. Zhuang, C. Ke, O. Voznyy, Y. Hu, Y. Li, W. A. Goddard III, B. Zhang, H. Peng, E. H. Sargent, *J. Am. Chem. Soc.*, **143**, 6482; DOI: 10.1021/jacs.1c00384.

*Received January 18, 2022;*
*in revised form April 7, 2022;*
*accepted April 19, 2022*